The International Journal of Advanced Manufacturing Technology (2019) 101:209–221
https://doi.org/10.1007/s00170-018-2892-y

ORIGINAL ARTICLE

Sensitivity study of hardness profile of 4340 steel disc hardened by induction according to machine parameters and geometrical factors

Mohamed Khalifa[1] · Noureddine Barka[1] · Jean Brousseau[1] · Philippe Bocher[2]

Received: 25 July 2018 / Accepted: 12 October 2018 / Published online: 31 October 2018

Abstract
An adequate induction heat treatment operation should always identify, previously, the probable temperature distribution and hardness profile behavior in specific regions of the treated component according to heating process parameters. This paper presents an analysis of the effects of some geometrical factor related to the component and the coil and machine parameters on temperature distribution and case depth of an AISI 4340 low-alloy steel disc heated by induction. A Comsol model was created, defined as a group of process parameters followed by a mesh study. A Matlab algorithm coupled to the simulation model was designed to handle a large number of simulations and export temperature profile data. The case depth is then interpolated from collected temperature data and a statistical analysis was developed to create the hardness prediction model. The experimental tests conducted under the same process parameters support the numerical model results and approve the simulation, the prediction modeling, and the statistical study.

Keywords Induction heating · Simulation · Experimental validation · Sensitive study · 4340 steel disc

1 Introduction

For many years, induction heating has shown its success in the metallurgical industry, his remarkable productivity, energy efficiency, and capacity to manipulate complex parts and various metal shapes has made it a popular tool in many industrial heat treatment applications like melting, injection molding, brazing, and surface hardening [1–3]. Steel hardening by induction is a widespread application of induction heating that uses heat generated by electromagnetic fields and induced currents with rapid cooling (quenching) to increase the surface hardness of the steel [4–6]. The process consists of creating high heat intensity at concentrated region on the surface of the metal part. An alternative current characterized by its intensity and frequency is supplied to an coil. A magnetic field, which generated immediately inside the coil, induces a current at the metallic part. This current creates heat due to Joule effect. As a result, the temperature rises at heated location up to austenitization point. Induction heating could be applied to a wide variety of shapes and sizes and requires no physical contact between the treated component and induction coil [7–9]. The AC-induced current flowing decreases its density from the surface toward the internal part of the part. As a result, the produced heat distribution will be concentrated from the surface into a specific internal distance known as the penetration depth. After quenching, a very hard martensitic structure will be created in the heated region defined from the surface up to the penetration depth.

The penetration depth is related essentially to current frequency, but other process parameters could also affect the depth of this concentrated region such as the machine and geometrical parameters. Machine parameters include current frequency

✉ Noureddine Barka
noureddine_barka@uqar.ca

Mohamed Khalifa
mohamed.khalifa@uqar.ca

Jean Brousseau
jean_brousseau@uqar.ca

Philippe Bocher
philippe.bocher@etsmtl.ca

[1] Département de mathématiques, d'informatique et de génie, Université du Québec à Rimouski, Rimouski, Québec G5L 3A1, Canada

[2] Département de génie mécanique, École de technologie supérieure, Montréal, Québec H3C 1K3, Canada

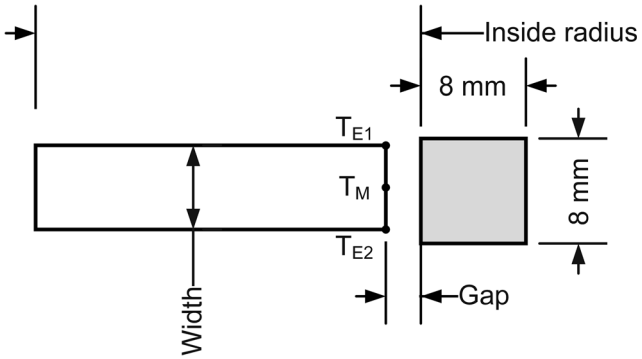

Fig. 1 Schematic representation of model components

(F_R), power density (P_M), and duration of the heating process (T_H) while geometrical parameters concern the shape, the size, dimensions, and relative positions of the treated object with an induction coil [1, 10]. The most important geometrical and machine parameters to consider in any induction heat application are the size of the treated object and its position beside the induction coil, where the most important machine parameters are current frequency, current density, and heating time [10, 11].

The study of induction heat treatment process has several difficulties at the simulation and experimental level. There is a difficulty in managing the complex electromagnetic and heating physics that includes several parameters and coupled physical phenomena. Moreover, material property data are not accurate and vary dissimilarly with the temperature. Measuring adequately the temperature and the machine current during heating process is a hard and challenging experimental task due to the quick heating rate. Researchers have proposed experimental and statistical methods that may be relevant to solve such problems. To make a good statistical study, it is necessary to choose the right parameters, to conduct well the experimental tests and to analyze adequately the obtained results. There is researchers that proposed this approach by simulation [10, 12, 13], by simulation with validation [14–16], and experimentation with planning strategy [17–20]. These studies are carry out to analyze various mechanical and thermal effect on a wide and different part shape, using electromagnetic induction process, in order to qualify or improve hardness, residual stress, deformation and final temperature distribution. Researchers made possible by simulation and/or experiments tests and mathematical models are analyzed generally with L_9 to L_{34} orthogonal array of combination parameters chosen by several methods including Taguchi method and synthesized with statistical model including regression and ANOVA techniques with verification by confirmation tests. The chosen combination parameters include either machine parameters, like power, heating time, and speed [11, 12, 15, 20], either machine and quenching parameters [18, 19], either machine parameters and metallurgical factors [17] or only geometrical part versus induction coil parameters [14]. This literature review demoted that there are no previous works that have combined both simulation and experimentation in statistical analyzes that include studying both of the machine parameters with the main geometric factors of the process. Therefore, the aim of this study is to develop a model that describes the hardness profile as a function of both geometrical and machine parameters based on a L_{81} orthogonal array. First, a 2D asymmetric model was developed, mesh studied, and then validated by experimental data. Second, a Matlab algorithm was developed and coupled with Comsol to carry out the simulations with different set of parameter's configurations. Finally, prediction equations of temperature profile and hardness depth were obtained by statistical analysis and partial experimental validation of extracted data.

Table 1 Simulation parameters with fixed machine power

Parameters	P_M	T_H	W_P	G_S	F_R
Level	66.5	0.5	6.5	2.5	200
Unit	kW	s	mm	mm	kHz

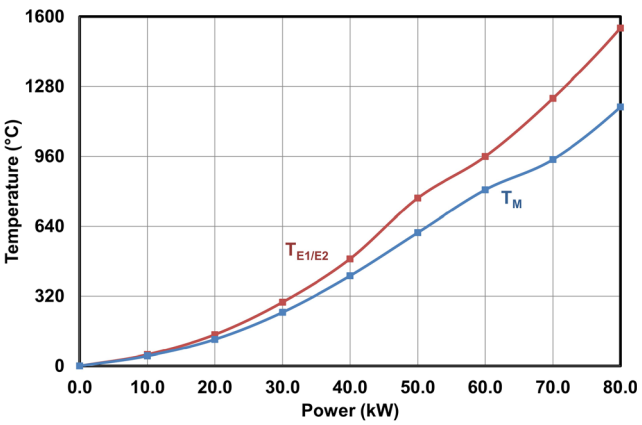

Fig. 2 Temperature evolution according machine power

2 Formulation

The formulation of induction heating process is described by an electromagnetic field (Maxwell's equations) in time varying form neglecting displacement field, which could be written as [1, 21]:

$$\text{Gauss}'\text{s law} \quad \nabla.D = \rho^{\text{charge}}(a) \tag{1}$$

Table 2 Validation test parameters

Parameters	P_M	T_H	W_P	G_S	F_R
Level	72.6	0.5	6.5	2.5	200
Unit	kW	s	mm	mm	kHz

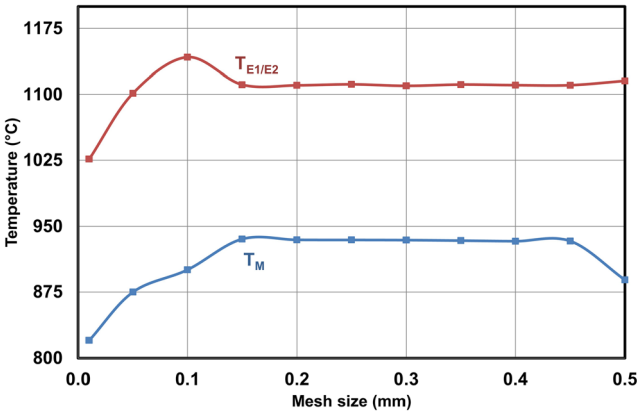

Fig. 3 Final temperature according the mesh size

$$\text{Faraday's law} \quad \nabla \times E = -\frac{\partial B}{\partial t} \tag{2}$$

$$\text{Gauss's law for magnetism} \quad \nabla . B = 0 \tag{3}$$

$$\text{Ampere's law} \quad \nabla \times H = J \tag{4}$$

With E, D, H, and B describes respectively the electric field intensity (V/m), electric flux density (C/m^2), magnetic field intensity (A/m), and magnetic flux density (T). ρ^{charge} is the electric charge density (C/m^3) and J is the conduction current density (A/m^2) and could be expressed by Ohm's law:

$$J = \sigma E \tag{5}$$

E and D, H, and B are related using Eqs. 6 and 7.

$$D = \varepsilon E \tag{6}$$

$$B = \mu H \tag{7}$$

With σ, ε, and μ represents, respectively, the electrical conductivity (S/m), permittivity (F/m), and magnetic permeability (H/m) of the material. These parameters are temperature dependent and the material is considered to be homogenous. Since B satisfies a zero divergence condition, equation becomes

$$B = \nabla \times A \tag{8}$$

where A is the magnetic vector potential. Since the field is time-harmonic, assumption of harmonically oscillating currents with single frequency make possible to write Eq. 2 in complex form such that

$$\nabla \times E = j\omega B \tag{9}$$

$$\nabla \times E = j\omega \, \nabla \times A \tag{10}$$

$$\nabla \times (E - j\omega A) = 0 \tag{11}$$

The curl is zero, the term $E - j\omega A$ will be equal to the gradient of a scalar function φ such that

$$\nabla\varphi = E - j\omega A \tag{12}$$

After multiplying with σ and inserting Eq. 5, Eq. 10 could be written as:

$$J = -\sigma\nabla\varphi - j\sigma\omega A \tag{13}$$

The current density could be written as the sum of an induced current J_i and an imposed external source current in the induction coil, J_0 such that:

$$J_i = -j\sigma\omega A \tag{14}$$

$$J_e = -\sigma\nabla\varphi \tag{15}$$

Inserting Eqs. 7, 8, and 11 in Eq. (4) gives

$$\frac{1}{\mu}(\nabla \times \nabla \times A) = J \tag{16}$$

$$\frac{1}{\mu}(\nabla \times \nabla \times A) = J_e - j\sigma\omega A \tag{17}$$

The resolution of Eq. 14 made it possible to determine the current density as a function of magnetic vector potential A which in turn could be deduced by resolving Eq. 17. The amount of heat generated inside the metal part due to joule heating is evaluated using the following equation.

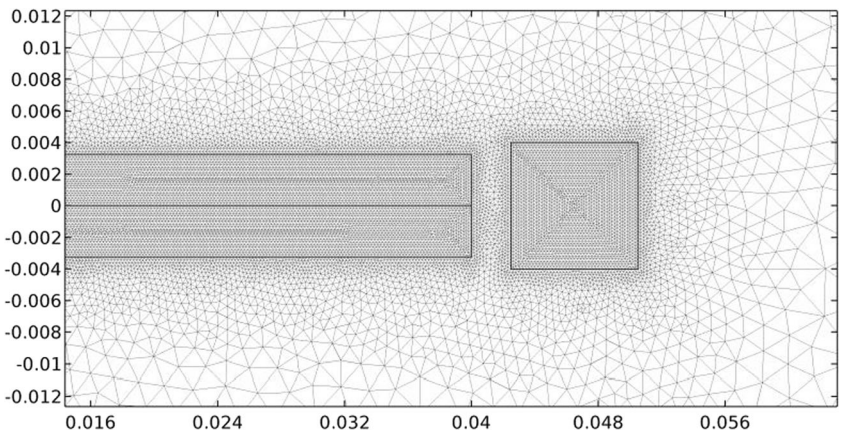

Fig. 4 Final mesh optimized by convergence study

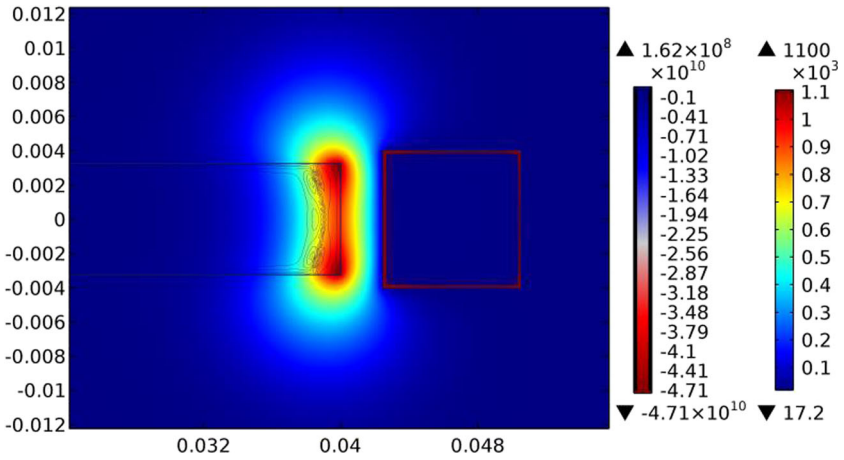

Fig. 5 Distributions of induction current (A/m^2) and temperature (°C)

$$Q_{\text{ind}}\,(W) = \int_{\text{v}} \frac{|J^2|}{\sigma}\, dV \tag{18}$$

The heat generated by induction is introduced into the heat equation in order to calculate the temperature distribution in the part. In induction heating, the heat transfer is described by Fourier's equation and it is given by [1]:

$$\rho C\,\frac{\partial T}{\partial t} = \nabla.(k\,\nabla \mathrm{T}) + Q_{\text{ind}} \tag{19}$$

where T is the temperature (K). ρ, C, and k are non-linear temperature-dependent properties and represent respectively the mass density (kg/m^3), the specific heat (J/kg K), and the thermal conductivity (W/(m K)) of material. A part of energy is lost by convection and radiation due to temperature differences between part and surrounding air. Convection and radiation heat flux losses q_c and q_r between the workpiece and open air are defined respectively as

$$q_c = h_c(T_s - T_a) \tag{20}$$

$$q_r = \varepsilon\sigma_s\left(T_s{}^4 - T_a{}^4\right) \tag{21}$$

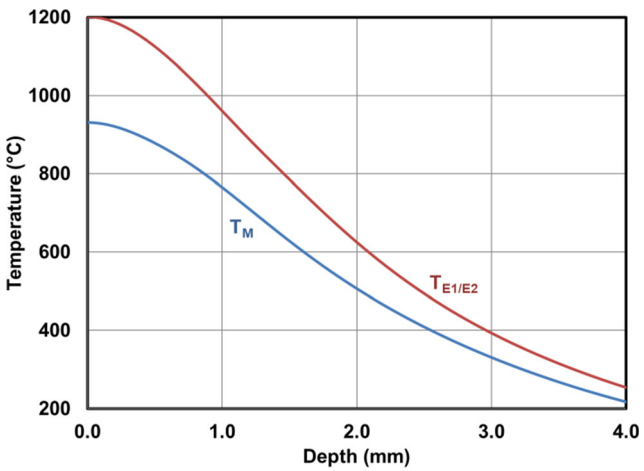

Fig. 6 Temperature distribution at the edge and middle profile

where h_c is the convection coefficient, ε is the emissivity, and σ_s is the Stefan-Boltzmann constant.

3 Simulation model

A disc made from low-alloy steel (AISI 4340) is placed inside 8 × 8 mm square coil. The geometrical parameters to be considered are the width of the disc (mm) and its relative distance with the coil (gap (mm)). The model is represented in Fig. 1. Due to geometry symmetrical properties, the model could be reduced from a 3D model into axisymmetric 2D model, this geometry reduction increase the numerical computation time and gives approximately the same results. Temperature distribution in the part is evaluated by defining three points, Tm is the points on the middle of the surface, and T_{E1} and T_{E2} are the point on the edge of outside surface. Due to symmetrical properties of the disc, the two edges will have the same temperature distribution so T_{E1} will be equal to T_{E2}.

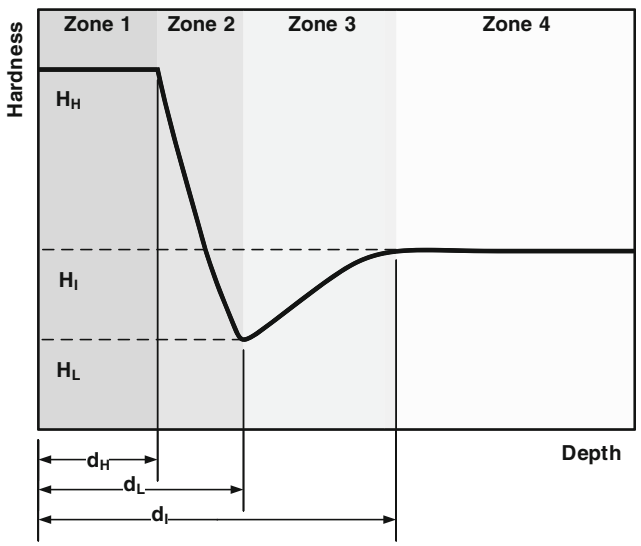

Fig. 7 Typical hardness profile by induction heating

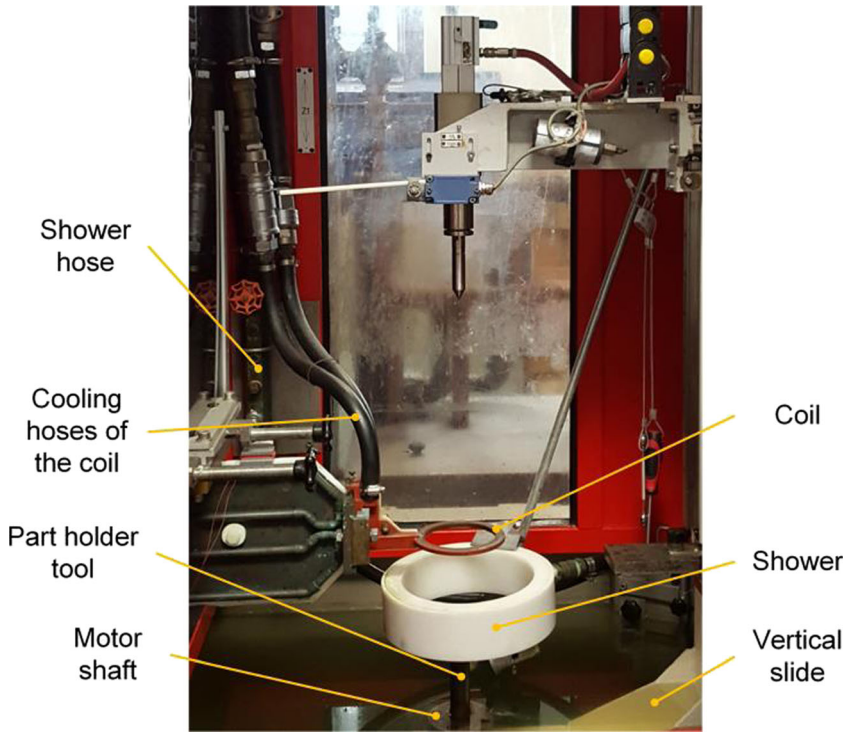

Fig. 8 Induction machine and operation system

3.1 Power under typical configuration

Using induction-heating systems to harden the part requires changing its surface layer microstructure by heating it to temperatures that are above or inside the austenitization range. The temperature distribution after heating will not be uniform between the surface layer and the inner portion of the disc, and it will decrease rapidly while getting closer to the surface middle and the disc center [7]. The mesh size is very refined and it is fixed at 0.2 mm that generates 33,677 elements and 135,072 degrees of freedom. The heating time (T_H) is fixed at 0.5 s and the width (W_P) is fixed at 6.5 mm. Finally, the gap (G_S) is fixed at 2.5 mm. The outer surface exactly into the austenite transformation temperature will not ensure that the heat will propagate sufficiently along the internal part of the part and that will have no effect in changing the surface microstructure inside the disc. Since the high frequency heating is only study, the frequency is fixed at 200 kHz. The last parameter to tune is the imposed current density (J_0). This parameter is replaced by the real machine power using the approximated ratio developed by

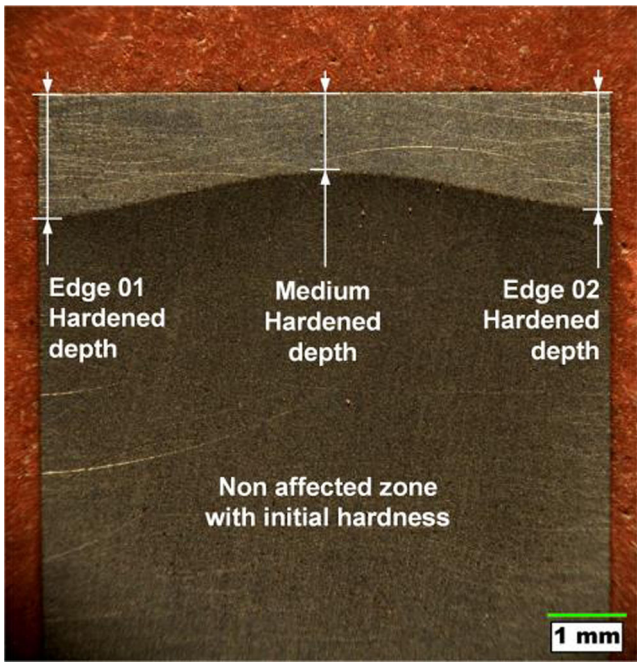

Fig. 9 Hardness profile obtained by experiments

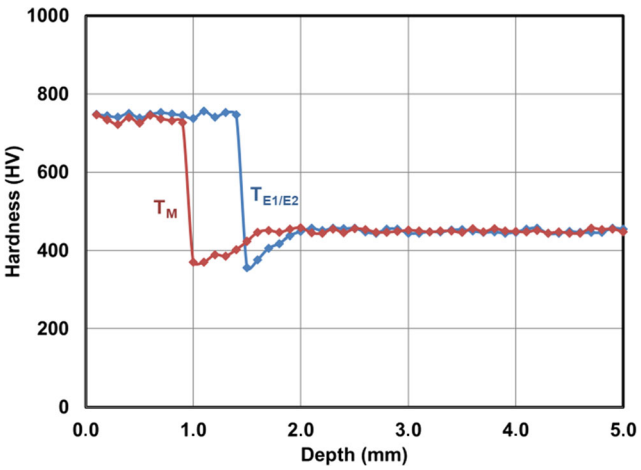

Fig. 10 Hardness curve on edge and middle obtained after the experimental test

Table 3 Stratching parameters and their levels

Parameters	P_M	T_H	W_P	G_S
Level 1	70	0.4	6.3	2.4
Level 2	72.5	0.45	6.5	2.5
Level 3	75	0.5	6.7	2.6
Unit	kW	s	mm	mm

Barka et al. [10]. Figure 2 shows the evolution of final temperature according the machine power. It is interesting to remark that the temperatures are identical at low power and the offset continues to increase to reach maximal value at 80 kW. The temperatures have a parabolic evolution and some variation caused by the material properties are occurred between 55 and 65 kW. To ensure that a transformation will occur inside the part, and that 100% austenite will be formed within the treated area, the temperature used for austenitization must be above A_{c3}, surface middle temperature of 900 °C will be considered sufficient to meet these conditions. Considering all geometrical and machine parameters, the most flexible input parameter is power delivered by the machine into the induction coil because it can be changed softly and precisely from the simulation software by the machine operator with no risk of error. All the machine and geometrical parameters, except the input power, will be fixed into reference level as shown in Table 2. The input power values vary from 10 to 100 kW in the simulation with a step of 10 kW and very smooth mesh size of 0.1 mm to see in which point the surface middle temperature T_M will exceed 900 °C.

The edge and middle temperatures increase with power and could attempt very high levels that exceed the melting point from 80 kW. The edge temperature increases faster than the middle temperature due to the edge effect phenomena. Edge temperature exceeds the value of 900 °C starting from 57 kW power machine value while middle temperature exceeds it with 66.5 kW input power value. The reference values are given in the Table 1.

3.2 Mesh convergence study

To determine the appropriate mesh size value, a mesh convergence study was carried out by Comsol. The default parameters of frequency, process duration, part width, the gap, and machine power were chosen in order to reach the austenitization point in the surface of the part ($T_M = 900$ °C). Figure 3 illustrates the evolution of temperature using the same machine parameters and geometrical factors according to meshing size. The truncation errors affect the evolution at the top of the value 0.45 mm, while the numerical errors affect this temperature down 0.15 mm.

Figure 4 shows the final configuration of optimal mesh obtained using the convergence study. Indeed, a simple section does not represent a good approximation of the problem since the induced currents are distributed at external surface.

3.3 Distribution of induced currents and temperature

Figure 5 shows the distributions of the total current density and the temperature after a heating time of 0.5 s in the case of high-frequency heating. The initial density of the current in the coil (J_0) is adjusted to also have a maximal temperature of 1100 °C. The currents are concentrated, in this case, on a thin layer in the edges of the coil and in the part because of the skin depth. The temperature profile is profounder at the edges than the middle plane since the currents are more concentrated at the corners of the coil. The preliminary results clearly show the presence of the both electromagnetic effects, the skin effect and the edge effect. These results also show that the temperature distributions are a direct consequence of the currents induced in the part and this profile has a considerable effect on the final hardness profile.

The temperature is at its maximum on the surface and decrease rapidly toward the disc center. Edge temperature is slightly higher than in the middle, but still both have the same temperature profile for every heating step time. In the HF case, the temperatures are distributed over a larger area on the edge

Table 4 Temperature at middle obtained by simulation (°C)

P_M (kW)		70	70	70	72.5	72.5	72.5	75	75	75
T_H (s)		0.4	0.45	0.5	0.4	0.45	0.5	0.4	0.45	0.5
G_S (mm)	W_P (mm)	Middle temperature (°C)								
2.4	6.3	898.69	932.71	990.54	929.15	991.98	1059.52	985.20	1055.49	1149.86
2.4	6.5	875.11	921.33	963.82	918.52	965.41	1051.26	951.35	1029.52	1077.01
2.4	6.7	863.52	901.28	966.58	919.76	966.56	1015.29	956.30	1014.84	1115.50
2.5	6.3	886.47	910.39	953.67	903.01	956.44	1007.69	941.00	1008.05	1092.41
2.5	6.5	878.42	891.80	931.04	889.07	932.74	982.96	928.18	979.81	1068.63
2.5	6.7	868.44	911.22	920.28	881.94	921.71	964.80	911.76	972.26	1033.97
2.6	6.3	843.64	868.30	934.02	866.08	907.10	965.83	897.91	960.29	1028.68
2.6	6.5	829.53	886.57	920.58	886.71	891.26	957.98	903.40	959.04	1006.20
2.6	6.7	842.04	881.34	883.10	879.11	898.37	941.02	890.88	937.82	986.56

Table 5 Temperature at edge obtained by simulation (°C)

P_M (kW)		70	70	70	72.5	72.5	72.5	75	75	75
T_H (s)		0.4	0.45	0.5	0.4	0.45	0.5	0.4	0.45	0.5
G_S (mm)	W_P (mm)	Edge temperature (°C)								
2.4	6.3	1146.41	1203.83	1271.65	1211.86	1288.32	1358.62	1294.99	1373.53	1452.56
2.4	6.5	1162.56	1193.67	1250.98	1201.92	1267.58	1355.85	1277.41	1346.76	1411.22
2.4	6.7	1146.21	1169.32	1260.99	1208.40	1284.44	1325.88	1281.10	1341.49	1428.63
2.5	6.3	1115.48	1183.61	1222.56	1181.22	1240.59	1298.45	1238.30	1314.41	1408.97
2.5	6.5	1104.81	1137.56	1200.39	1144.54	1217.47	1274.61	1222.68	1285.78	1398.39
2.5	6.7	1088.32	1121.54	1189.17	1133.55	1203.45	1260.54	1212.70	1284.79	1354.79
2.6	6.3	1109.42	1099.50	1178.32	1107.12	1186.28	1245.26	1190.45	1258.63	1331.16
2.6	6.5	1094.25	1115.09	1165.46	1129.17	1172.73	1250.44	1196.95	1273.14	1313.49
2.6	6.7	1083.84	1109.23	1152.32	1117.43	1190.37	1227.27	1183.06	1239.37	1297.15

compared to the middle plane. In addition, the maximum temperature values record a clear offset of 280 °C between the edge and middle (Fig. 6). The heated zone on the edge reaches 260 °C at a depth of 4 mm and 230 °C at the middle plane at the same depth. The temperature curve following the depth at the end of heating makes it possible to predict the hardened region and suggests that the region near the edges is transformed into hard martensite while that at the middle plane of the part does not reach the temperature necessary to martensitic transformation. Similarly, if the temperature of 600 °C is assumed a legitimate assumption, the depths affected are 2.1 mm at the edge and 1.6 mm at the middle plane.

In order to interpret a temperature profile into a hardness profile, the critical austenitization temperatures Ac_1 and Ac_3 that characterize the heated region after 0.5 s must be considered. Thus, the temperature Ac_1 characterizes the onset of formation of the austenite while the temperature Ac_3 characterizes the end of the martensite returned (initial microstructure) and all the regions heated above this temperature are austenitized to 100%. The region between the Ac_1 and Ac_3 temperatures is a mixture of austenite and unconverted returned martensite. The final temperature distribution has a direct impact on the hardness profile in the part and its evolution as a function of depth (surface hardness and hardened depth). If the assumption that all regions heated above Ac_3 (100% austenite) become martensite lasts after cooling and that this temperature for a heating time of 0.50 s is approximated to 850 °C, it is possible to appreciate the hardened depth for both the MF and HF cases on the edge and the middle plane.

Table 6 Percent contribution of parameters on edge and middle temperatures

Parameters	Edge	Medium
P_M	45.26%	32.92%
T_H	31.84%	40.05%
W_P	1.11%	2.44%
G_S	18.25%	17.48%
$P_M \times T_H$	0.92%	2.12%
$P_M \times G_S$	Insignificant	0.97%
Error	2.61%	4.07%

3.4 Case depth versus temperature curves

The simulated case depth is deduced from critical transformation temperature distribution across the disc assuming that a rapid cooling (quenching) is done perfectly after the heating process to form a new and hard martensitic microstructure. The transformation temperatures are identified to be the critical temperature Ac_1 (825 °C) corresponds to the apparition of first austenite germs. Ac_3 (850 °C) corresponds to the temperature at which the first germs of austenite appear. Finally, the critical temperature (T_r) fixed at 640 °C is assumed to be the lowest temperature that affects the part microstructure [22]. In fact, this temperature characterize the depth where the hardness recovers the initial value in the part core. To retrieve the corresponding critical depth d_i for each critical temperature Ac_1, Ac_3, and Tr, a linear interpolation function was used between the closest higher temperature and closest smaller temperature values with their corresponding depth values from the simulation results (Fig. 7). High surface hardness is related to martensite formation, which in turn is dependent upon heating to austenite range and cooling rate. Therefore, the simulation results and temperature distribution could reveal the shape and size of the hardened region and case depth.

Table 7 Percent contribution of parameters on edge depths

Parameter	d_H	d_L	d_I
P_M	35.39%	34.54%	28.22%
T_H	48.3%	49.6%	59.26%
W_P	0.74%	0.73%	0.69%
G_S	12.91%	12.48%	9.47%
Error	2.66%	2.66%	2.36%

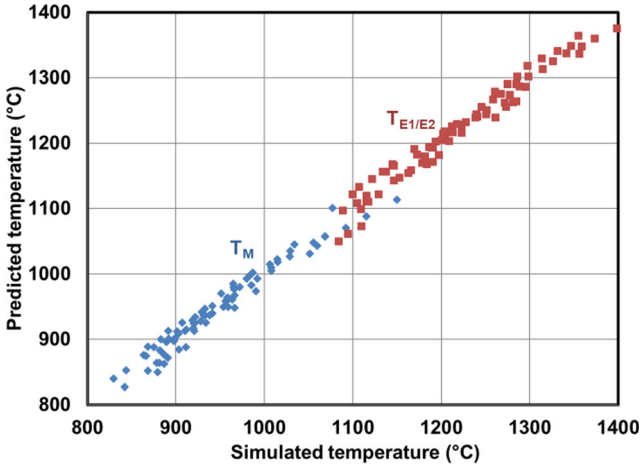

Fig. 11 Simulated temperatures versus predicted temperature at middle and edges

3.5 Preliminary experimental validation

Experimental validation tests are performed using the induction machine located at the École de Technologie Supérieure (Montreal, Canada). This machine contains solid state converters (10 kHz) and thyristor radio frequency generator (200 kHz). The first one provides a maximum power of 550 kW and the second generator delivers a maximum power of 450 kW. This machine is capable to control both frequencies using the sequential double frequency heating concept and it is a numerically commanded using two numerical axes (Fig. 8).

The first test was done under the following machine parameters and geometry configuration. This tuning data (Table 2) is used to validate the first model developed by simulation.

The hardness profile at the edge and middle of the disc obtained by the previous configuration is shown in Fig. 9.

It is important to note that the hardness profile is not uniform across the part section. Due to the edge effect, the magnetic field is concentrated more at the edges than in the middle. This fact generate a deep layer with important concentrated currents that heat more the edges than the middle. After been transformed to austenite, the regions are transformed to thin martensite. Due to lack temperature diffusion and skin effect, the non-affected zone toward the center of the disc remains with its initial hardness value and no structural and phase change occurs in this region.

As illustrated in Fig. 10, the hardness curve measured at the edge and the middle has a typical hardness profile as expected with significant difference on critical depth for both positions, due to edge effect. It can be shown that a conformity in the shape exists between simulation and experimental tests for both edge and middle profile. One can remark that the hardness at the surface are slightly the same at the middle and the edges. It is also interesting to observe that the low hardness is about 370 HV and the over-tempered zones have the same width in both cases.

4 Sensitive study — Temperatures

A sensitivity study was performed to determine the effects of geometrical (G_S and W_P) and machine parameters (P_M and T_H) with a fixed HF frequency (200 kHz). In order to avoid reaching melting point temperature during the heating process especially at the edge, which refers to the maximum configuration parameters and considering that temperature in the middle surface must reach at least austenitization point at the end of the process, which refers to the minimum configuration parameters, a range of parameters between maximum and minimum group values are chosen based on Taguchi method and verified by simulation (Table 3). Each of the four independent variables will be calculated in three levels, giving 81 possible configurations and corresponding to the 81 simulations.

The classical technique for handling simulation is exploited manually, but since the number of configuration is great and the mesh is very condensed, this kind of manual work of input and result extraction will take a very long time [10]. To optimize this time and effort problem, all 81 simulations were automatized by writing a MATLAB code coupled with a Comsol built-in functions. This automated method solution reduced the calculation and results extraction into just 6 h even with a very condensed mesh size. Results were the temperature distribution alongside the edge and the middle plan of the heated disc. Statistical analysis was performed to analyze the effect of these independent geometrical and machine parameters on temperature distribution and hardness profile.

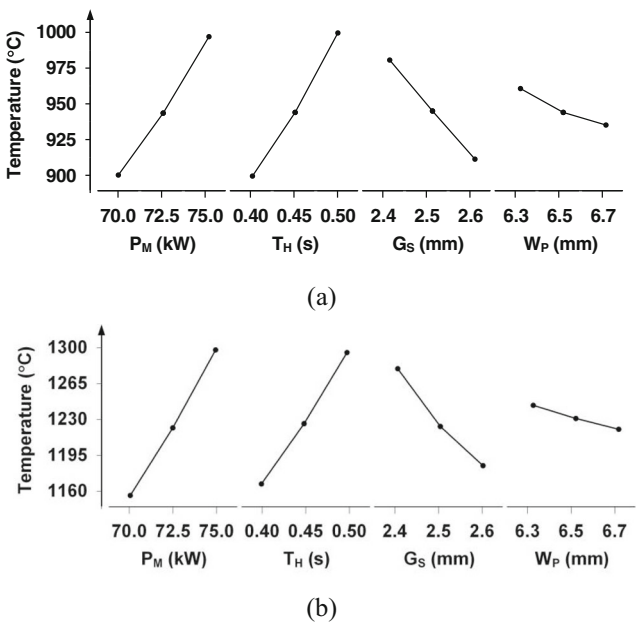

Fig. 12 Effect of geometry factors and machine parameters on temperature, **b** middle and **a** edge

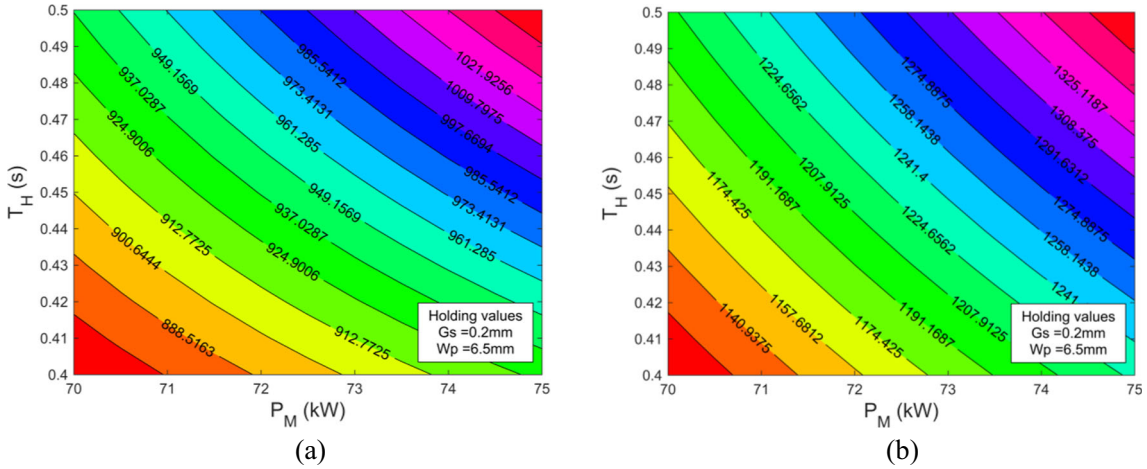

Fig. 13 Response surface methodology of surface temperature in the **a** middle and at the **b** edge

4.1 Simulation data

The following data presented in Tables 4 and 5 are extracted from results simulations and summarize the temperature values at middle and edge of the part. It can be shown that final process temperatures are above the austenitization temperature Ac_3 as desired and respects the non-melting condition for middle region but it can be reached at the following condition at the edge (75 kW, 0.5 s, $G_S = 2.4$ mm and $W_P = 6.3$ mm), and the following configuration is the extreme case and temperature is at its highest values.

4.2 Contributions

After performing statistical analysis on simulation results, the contribution of each factor on the final temperature could be interpreted. Table 6 shows the contribution factor percentage for each parameter on edge and middle temperatures. It can be shown that T_E and T_M are highly influenced by the power and the heating time. Both contribute in more than 70% on final temperature values. Power has more effect on the edge (45.62%) than the middle temperature (32.92%) while heating time has more contribution on middle temperature (40.05%) than edge temperature (31.84%) (Table 6). The gap has an important effect and it is involved in more than 17% for both middle and edge temperatures. The part width has no significant effect and could be neglected.

Table 8 Percent contribution of parameters on edge depths

Parameter	d_H	d_L	d_I
P_M	26.98%	30.6%	24.41%
T_H	50.01%	49.46%	60.45%
W_P	2.54%	1.98%	2.61%
G_S	16.93%	15.01%	9.61%
Error	3.54%	2.95%	2.93%

4.3 Simulated versus predicted temperatures

One goal of this study is to find a model that gives the most valid prediction of the edge and surface temperature given the geometrical and machine parameters. The ANOVA statistical study gives equation that describes the predicted relationship between temperatures in function with all other parameters for the edge and the middle point. The fitness of the model should be examined and evaluated. Experimentally, it is a difficult task to measure instantly the temperature distribution across the part section as the process happens very quickly. Figure 11 presents the scatter plot for T_E and T_M. It is clear that for each simulated response value, the predicted value is at the diagonal line, due to the low value of the residuals errors. Consequently,

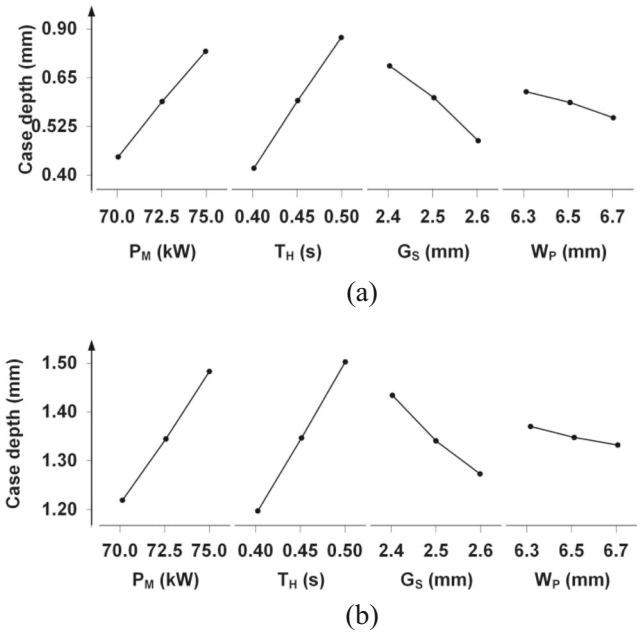

Fig. 14 Effect of geometry factors and machine parameters on case depth, **b** middle and **a** edge

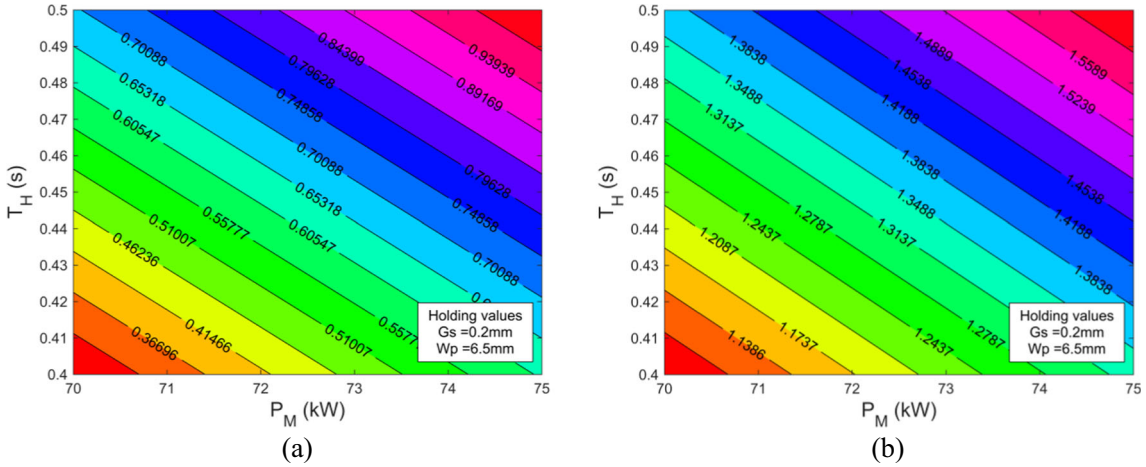

Fig. 15 Response surface methodology of case depth in the **a** middle and at the **b** edge

for each value of temperatures, the predicted and simulated curves are nearly identical, which explains the good agreement between the predicted and the measured values. The linear fitting criteria that the prediction equation is able to assume a satisfactory level of accuracy with simulation results.

After eliminating the non-significant terms, the empirical relationship between the temperatures at th edge and in the middle of the heated part by Eqs. 22 and 23. The equations present an approximate model based on linear regression and allows the evaluation of the temperature according the machine parameters and the geometrical factors.

$$T_E = 3415 - 16.66xP_M - 6159xT_H - 57.1W_P - 462.8xG_S + 101.8xP_MxT_H \quad (22)$$

$$T_M = -2709 + 61.3xP_M - 7282xT_H - 62.76xW_P + 2402xG_S + 114.5xP_MxT_H - 37.76xP_MxG_S \quad (23)$$

4.4 Effects of machine parameters on temperatures

The average effect of geometrical and machine parameters on the final edge and machine temperature are presented in Fig. 12a, b. Each factor contribute by its own degree on the temperature. The power and heating time have the biggest influence. An increase of 2.5 kW in machine power contribute to an increase of 80 °C in edge temperature and 40 °C on middle temperature. A short increase on the heating time (0.05 s) leads to an important temperature rise for both points, at about 50 °C increase on the edge temperature and 40 °C on middle temperature. Geometrically, the temperature decrease significantly when increasing the gap. A 0.1 mm of gap variation leads to a temperature drop of about 60 °C on the edge and about 40 °C at the middle. The part width (W_P) has no significant influence of the final temperature distribution. A 0.1 mm of W_P variation decrease the temperature by 10 °C on the edge and 20 °C on the middle. It is important to note that, unlike other factors, part width has more influence on middle temperature than the edge temperature.

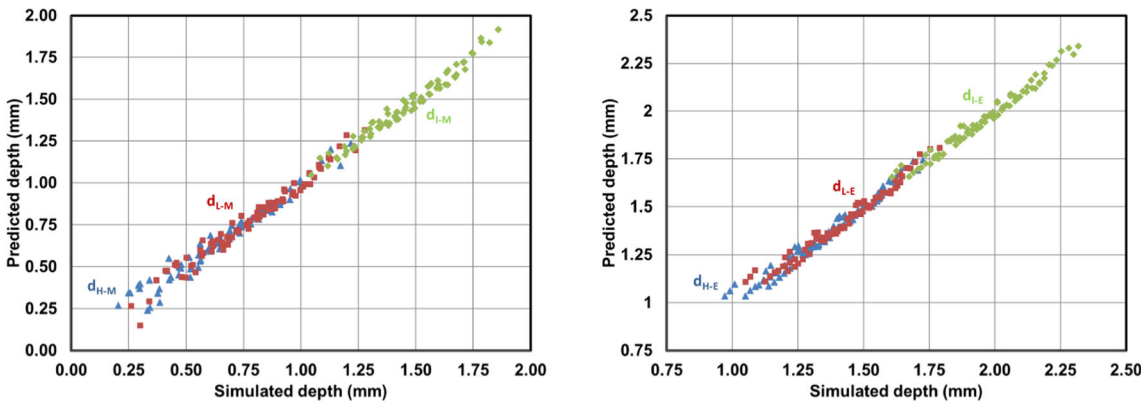

Fig. 16 Simulated depths versus predicted depths at middle (**a**) and in edges (**b**)

Table 9 Experimental validation tests

Parameters	P_M	T_H	W_P	G_S	F_R
Test 2	42.9	1	6.5	2.5	200
Test 3	56.1	1	6.5	2.5	200
Unit	kW	s	mm	mm	kHz

The response surface methodology (RSM) given by ANOVA analysis is a fast and powerful way to predict the final temperature in function with the process parameters. Edge and middle temperature are presented according to the power and heating time values. The gap and the part width are maintained in typical centered values of 2.5 mm and 6.5 mm. It can be shown that for both points, temperature has a parabolic profile and increases proportionally with the power and heating time. Figure 13 illustrates the RSM obtained at the edge and in the middle of the heated part.

5 Sensitivity study — Case depths

The final temperature distribution is converted to hardness curve using Matlab code. In fact, the temperatures according to the depth at the middle and at the edge are converted to hardness curve as explained using Fig. 7. After interpolating the critical depth values d_H, d_L, and d_I corresponding respectively to critical temperatures Ac_3, Ac_1, and Tr, statistical analysis was done to deduce the contribution of geometrical and machine parameters on these simulated critical depth. According to statistical analysis (Tables 7 and 8), the most important factor having effect on the case depth is the heating time with about 50% contribution percentage. The machine power contributes significantly on the final case depth with about 35.4% at the edge and 27% on middle. The influence of the part width is insignificant with about 0.74% at edge and 2.5% on middle. However, the gap has an important effect on the case depth with about 13% contribution percentage on the edge and 17% contribution percentage in the middle. The analysis result also demonstrates that the geometrical factors contribute much more in the middle than at the edge.

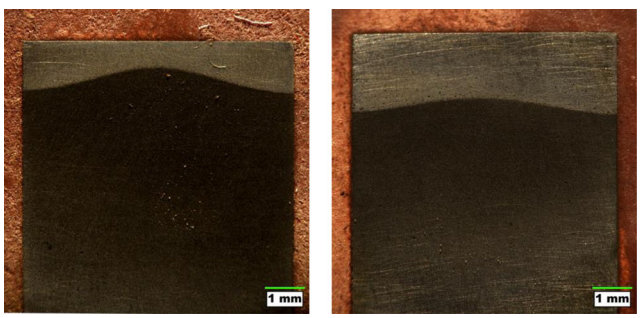

(a) (b)

Fig. 17 Hardness profile obtained by Test 2 (**a**) and Test 3 (**b**)

5.1 Effects of machine parameters on case depths

Figure 14 represents respectively the case depth in the edge and at the middle layer after heating and assuming a perfect quenching process in function of machine power and heating time, maintaining the part width and gap in their centered value. It is clear that case depth has a linear profile and increase in the same rate with time and power. As is known, due to edge effect, the case depth has bigger values on edge than in the middle layer. The case depth value is up to 1.62 mm in the edge and 1.04 mm in the middle.

Figure 15 describes the average effect of geometrical and machine parameters on the case depth. The response of case depth is analogous to temperature distribution and the effects of variant parameters on it are similar. A small increase in the machine parameters increases the case depth rapidly while increasing the geometrical parameters values have the opposite effects. The case depth is higher under these conditions (75 kW, 0.5 s, $G_S = 2.4$ mm and $W_S = 6.3$ mm), and lower under the following configuration (70 kW, 0.4 s, $G_S = 2.6$ mm and $W_S = 6.7$ mm).

5.2 Simulated versus predicted case depths

ANOVA analysis gives the following equations describing critical case depths d_H, d_L, and d_I in function of geometrical and machine parameters. It can be shown from Fig. 16 that the predicted and simulated depth values are strongly correlated. The next part will examine the correctness of the predicted model equations with experimental results. Figure 16 presents the scatter plot for case depths at edges and in middle locations. It is clear that for each measured response value, the predicted value is close to the diagonal line, due to the low value of the residuals of the predicted values. For each value of case depths, the predicted and measured curves are nearly identical, which explains the good agreement between the predicted and the measured values.

6 Final experimental validation

Experimental validation tests were done under the following configurations, illustrated in Table 9. The obtained results demonstrate that simulation combined to practical tests can be used advantageously for the development of recipes intended to develop mechanical components by induction (Fig. 17).

Figure 18 illustrates predicted and measured hardness curves corresponding to test 2. Results show that the prediction model and experimental data fit together and that error

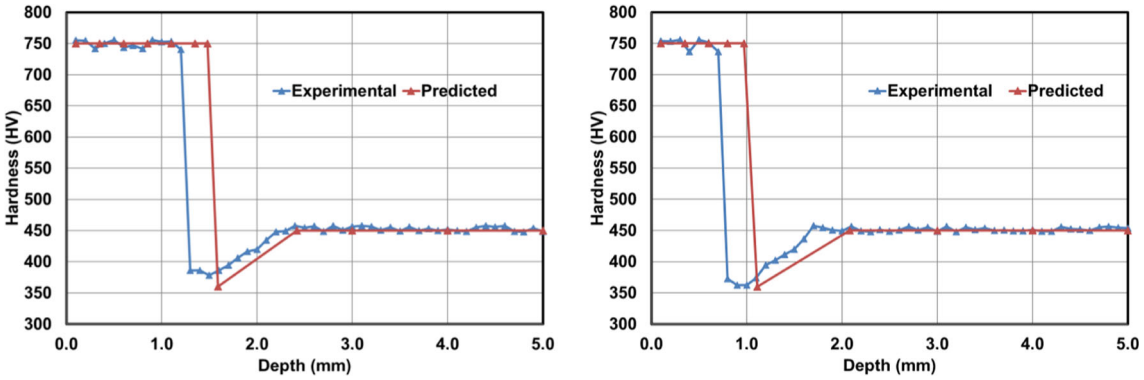

Fig. 18 Predicted and measured hardness curves for Test 2, edge (**a**) and middle (**b**)

between the three curves is relatively low and is about 5 up to 19%. The marge of error is smaller for experimental tests where input power and heating time values are close to those used in the simulation. Still, the mathematical model is reliable for predicting the effect of input parameters on critical depths and to predict the over-tempered zone profile.

7 Conclusion

The main feature of this study is the great number of simulation done in order to create a reliable and acceptable model that predicts the effect of geometrical and machine parameters on the hardness depth of an AISI 4340 low-alloy steel disc heated by induction. First, a 2D axis-symmetric model was developed using Comsol that couple electromagnetic and thermal heating to create and design the temperature distribution on the disc after induction heating process. A power and mesh convergence study was carried out to identify and select the best and typical machine, geometry configuration for the simulation work. A MATLAB algorithm development has greatly reduced and optimized the simulation time. Statistical analysis using ANOVA has demonstrated the on the case depth, which values were extracted from the final temperature distribution, has shown great concordance between the mathematical model and experimental results, with an average error less than 15%. In summary, the obtained mathematical model implies a very good ability to predict the hardness and the over tempering zone when the experimental values are close to simulation parameters input. It is interesting also to expand the developed MATLAB algorithm and mathematical models on other work and studies such as optimization problems and working on complex geometries such as spurs and helical gears.

References

1. Rudnev V, Loveless D, Cook R (2017) Manufacturing engineering and materials processing. In: Handbook of Induction Heating, 2nd edn. Boca Raton, CRC Press, Taylor & Francis Group xxi, 749 pages
2. Guerrier P et al (2015) Three-dimensional numerical modeling of an induction heated injection molding tool with flow visualization. Int J Adv Manuf Technol 85(1–4):643–660
3. Guo X et al (2015) Numerical simulations and experiments on fabricating bend pipes by push bending with local induction-heating process. Int J Adv Manuf Technol 84(9–12):2689–2695
4. Han Y, Yu E-L, Zhao T-X (2016) Three-dimensional analysis of medium-frequency induction heating of steel pipes subject to motion factor. Int J Heat Mass Transf 101:452–460
5. Hömberg D, Liu Q, Montalvo-Urquizo J, Nadolski D, Petzold T, Schmidt A, Schulz A (2016) Simulation of multi-frequency-induction-hardening including phase transitions and mechanical effects. Finite Elem Anal Des 121:86–100
6. Achraf S et al (2016) Temperature history modelling and validation of fast induction hardening process. In: HES-16 heating by electromagnetic sources. U.d.S.d. Padova, Editor, Padua
7. Barglik J, Smalcerz A, Przylucki R, Doležel I (2014) 3D modeling of induction hardening of gear wheels. J Comput Appl Math 270: 231–240
8. Munikamal T, Sundarraj S (2012) Modeling the case hardening of automotive components. Metall Mater Trans B 44(2):436–446
9. Wen H, Han Y (2017) Study on mobile induction heating process of internal gear rings for wind power generation. Appl Therm Eng 112:507–515
10. Barka N, Bocher P, Brousseau J (2013) Sensitivity study of hardness profile of 4340 specimen heated by induction process using axisymmetric modeling. Int J Adv Manuf Technol 69(9–12):2747–2756
11. Kochure PG (2012) Mathematical modeling for selection of process parameters in induction hardening of EN8 D steel. IOSR Journal of Mechanical and Civil Engineering 1(2):28–32
12. Barka N (2017) Study of the machine parameters effects on the case depths of 4340 spur gear heated by induction—2D model. Int J Adv Manuf Technol 93:1173–1181
13. Candeo A, Ducassy C, Bocher P, Dughiero F (2011) Multiphysics modeling of induction hardening of ring gears for the aerospace industry. IEEE Trans Magn 47(5):918–921
14. Huang M-S, Huang Y-L (2010) Effect of multi-layered induction coils on efficiency and uniformity of surface heating. Int J Heat Mass Transf 53(11–12):2414–2423

15. Bae K-Y, Yang YS, Hyun CM, Cho SH (2008) Derivation of simplified formulas to predict deformations of plate in steel forming process with induction heating. Int J Mach Tools Manuf 48(15): 1646–1652
16. Barka N, Chebak A, el Ouafi A, Jahazi M, Menou A (2014) A new approach in optimizing the induction heating process using flux concentrators: application to 4340 steel spur gear. J Mater Eng Perform 23(9):3092–3099
17. Kristoffersen H, Vomacka P (2001) Influence of process parameters for induction hardening on residual stresses. Mater Des 22:637–644
18. Besserer H-B, Dalinger A, Rodman D, Nürnberger F, Hildenbrand P, Merklein M, Maier HJ (2016) Induction heat treatment of sheet-bulk metal-formed parts assisted by water-air spray cooling. Steel Res Int 87(9):1220–1227
19. Dmytro R et al (2012) Investigation of the surface residual stresses in spray cooled induction hardened gearwheels. Int J Mater Res 103(1):73–79
20. Kochure PG, Nandurkar KN (2012) Application of taguchi methodology in selection of process parameters for induction hardening of EN8 D Steel. International Journal of Modern Engineering Research (IJMER) 2(5):3736–3742
21. Jin J (2002) The finite element method in electromagnetics. John Wiley & Sons Inc., New York
22. Barka N, el Ouafi A, Bocher P, Brousseau J (2013) Explorative study and prediction of overtempering region of disc heated by induction process using 2D axisymmetric model and experimental tests. Adv Mater Res 658:259–265